Ocean Sci. Discuss., 9, 3431–3449, 2012
www.ocean-sci-discuss.net/9/3431/2012/
doi:10.5194/osd-9-3431-2012

Ocean Science Discussions

A modelling study of the hydrographic structure of the Ross Sea

M. Tonelli[1], **I. Wainer**[1], **and E. Curchitser**[2]

[1]Oceanographic Institute, University of Sao Paulo, Praca do Oceanografico, 191, Sao Paulo, SP 05508-120, Brazil
[2]Institute of Marine and Coastal Science, Rutgers University, 71 Dudley Rd., New Brunswick, NJ 08901, USA

Received: 15 October 2012 – Accepted: 19 October 2012 – Published: 6 November 2012

Correspondence to: M. Tonelli (mtonelli@usp.br)

Published by Copernicus Publications on behalf of the European Geosciences Union.

Abstract

Dense water formation around Antarctica is recognized as one of the most important processes to climate modulation, since that is where the linkage between the upper and lower limbs of Global Thermohaline Circulation takes place. Assessing whether these processes may be affected by rapid climate changes and all the related feedbacks may be crucial to fully understand the ocean heat transport and to provide future projections. Applying the Coordinated Ocean-Ice Reference (CORE) normal year forcing we have run a 100-yr simulation using Regional Ocean Model System (ROMS) with explicit sea-ice/ice-shelf thermodynamics. The normal year consists of single annual cycle of all the data that are representative of climatological conditions over decades and can be applied repeatedly for as many years of model integration as necessary. The experiment employed a circumpolar variable resolution (1/2° to 1/24°) grid reaching less than 5 km over the inner continental shelf. With Optimum Parameter Analysis (OMP) the main Ross Sea (RS) water masses are identified: Antarctic surface water (AASW), circumpolar deep water (CDW), shelf water (SW) and ice shelf water (ISW). Current configuration allows very realistic representation, where results compare extremely well to the observations.

1 Introduction

The ocean plays a significant role in modulating the global climate transporting heat from lower latitudes to polar regions through Global Thermohaline Circulation (THC; a.k.a. Conveyor Belt), which consist of an upper warm limb and cold deep one (Rintoul, 1991). The linkage of these two branches occurs at specific places around the polar regions, where the warmer limb releases heat to the atmosphere causing the surface water to lose buoyancy and to become denser. This is enhanced by the brine rejection due to sea-ice formation, resulting in cold water sinking and leading to the formation of the deep branch of the THC (Gordon, 1986).

OSD
9, 3431–3449, 2012

The Southern Ocean (SO) appears as a key region driving that system, since unique exchange processes and water transformation over the Antarctic continental shelf are responsible for the formation of the Antarctic Bottom Water (AABW); one of the main components of the THC's lower limb (Orsi et al., 2001, 2002). The main sources of deep waters in the SO are the Weddell Sea (WS) and the Ross Sea (RS), and the latter one is the formation site of two main AABW components: the high salinity shelf water (HSSW) and the ice shelf water (ISW; Jacobs, 2004; Bergamasco et al., 2004). HSSW production results from the extensive brine rejection in the RS polynya, while ISW is formed under the Ross Sea Ice Shelf (RIS) by means of basal melting. They interact under the RIS to become the densest water masses in the SO and flow towards the the continental shelf break to interact with the Circumpolar Deep Water (CDW), branched off from the Antarctic Circumpolar Current (ACC) into the cyclonic Ross Gyre (RG), producing the AABW (Jacobs, 2004; Assmann et al., 2003; Bergamasco et al., 2004). A representative scheme of the circulation under the RIS is shown on Fig. 1, as described by Smethie et al. (2005).

1.1 Ross Sea

Facing the Pacific sector of the SO, the RS is approximately centered at 180° W with a conic shaped area covering about $5 \times 105\,km^2$ between Cape Adare to Cape Colbeck. Although the average depth is 500 m, there are depressions that reach 1200 m and behave as dense waters reservoirs, since the shelf break represents the 700 m isobath (Budillon et al., 2003). The ACC follows the continental slope carrying the CDW from east to west and acts as the northern oceanographic boundary of the RS, as the CDW, after being captured by the RG, will be the only heat source to shelf waters strongly influencing the thermohaline circulation of this basin (Budillon and Spezie, 2000; Budillon et al., 2003).

Another important RS physical feature results from the strong katabatic winds pushing the newly formed ice offshore on the western side of the Ross Sea: the Terra Nova Bay polynya, whose annual recurrence provides salt fluxes large enough to increase

OSD
9, 3431–3449, 2012

the water column salinity and to form the HSSW (Bromwich and Kurtz, 1984; Kurtz and Bromwich, 1985; Jacobs, 2004; Budillon and Spezie, 2000; Bergamasco et al., 2004). The HSSW occupies the lowest layers flowing beneath the RIS to reach the basal ice and mix producing ISW. The newly formed ISW along with the HSSW that did not flow under the RIS will then flow northward to mix with the CDW at the shelf break producing deep and bottom waters (Jacobs et al., 1970; Gordon and Tchernia, 1972; Budillon et al., 1999; Bergamasco et al., 2002a). These processes make HSSW and ISW the most important shelf waters of the RS involved in the formation of the AABW and the deep ocean ventilation.

The low salinity shelf water (LSSW) appears at intermediate depths in the Central Eastern Ross Sea and is believed to result from the interaction between the Antarctic surface water (AASW) and subsurface waters (Jacobs, 2004; Assmann et al., 2003; Bergamasco et al., 2004; Muench et al., 2009). At surface layers, AASW is highly influenced by atmospheric oscillations and sea ice (Jacobs, 2004).

Thus the RS presents a complex, very regional hydrographic structure that is yet crucial for the large scale density-driven circulation. Modelling the RS and its deep water mass is a challenge and necessary taste in order to understand the role of southern oceans on climate change.

2 Model description

For this investigation we have used the Regional Ocean Model System (ROMS); a free-surface, terrain-following, hydrostatic primitive equations ocean model (Song and Haidvogel, 1994). All 2-D and 3-D equations are time-discretized using a third-order accurate predictor (Leap-Frog) and corrector (Adams–Molton) time-stepping algorithm. In the horizontal, the primitive equations are evaluated using boundary-fitted, orthogonal curvilinear coordinates on a staggered Arakawa-C grid. In the vertical, the primitive equations are discretized over variable topography using stretched terrain-following

OSD
9, 3431–3449, 2012

coordinates (Song and Haidvogel, 1994). More detailed descriptions may be found in Budgell (2005) and Wilkin and Hedstrom (1998).

2.1 Experiment setup

The simulation domain consists of a periodic circumpolar grid between 85.5° S and 30° S with variable horizontal resolution, reaching less than 5 km over the continental shelf (Fig. 2). It has a 1/2° zonal resolution and a varying meridional resolution which gradually increases from 1/2° at lower latitudes to 1/24° at the southernmost boundary, resulting in 722 × 309 grid cells. There are 40 terrain-following vertical levels with higher resolution near surface and bottom.

For the 3-D momentum advection a 4th order centered scheme is applied in the horizontal and in the vertical. For tracers, a 3rd order upstream horizontal and 4th order centered vertical advection schemes are applied. Biharmonic horizontal mixing of momentum and tracers is used in which the viscosity and diffusivity depend on the grid spacing. Quadratic bottom stress, with a coefficient of 3.0×10^{-3} was applied as a body force over the bottom layer. The vertical momentum and tracer mixing were handled using the KPP mixing scheme. For computational efficiency, ROMS uses a split-explicit time-stepping scheme in which external (barotropic) and internal (baroclinic) modes are computed separately. The external and internal time step were set to 0.75 and 30 min, respectively in compliance with the Courant, Friedrichs and Lewy (CFL) criterion.

A dynamic-thermodynamic sea-ice module is coupled to the ocean model, having both of them the same grid (Arakawa-C) and time step and sharing the same parallel coding structure (Budgell, 2005). The sea-ice dynamics is based on elastic-viscous-plastic (EVP) rheology (Hunke and Dukowicz, 2002). The sea-ice thermodynamics follows Mellor and Kantha (1989). Two ice layers and a single snow layer is used in the sea-ice module to solve the heat conduction equation. The salt flux underneath the sea-ice is a function of the basal melting or freezing which is controlled by the difference between the water-sea-ice heat flux and the sea-ice-atmosphere conductive heat flux (Holland and Jenkins, 2001). A thermodynamic ice shelf parameterization is included

OSD
9, 3431–3449, 2012

to consider the ice shelves effects on ocean circulation and water mass formation. The ice shelf has a static morphology where thickness and extent do not change. Under the ice shelves, the upper boundary conforms to the ice shelf base and the atmospheric contributions to the momentum and buoyancy fluxes are set to zero. The heat and salt fluxes are calculated as described in Dinniman et al. (2007) with the modification that the heat and salt transfer coefficients are functions of the friction velocity (Holland and Jenkins, 1999).

Two topographic surfaces must be defined for this model configuration: the bottom of the water column and, where necessary, the depth below mean sea level of the ice shelf thickness. Bottom topography was constructed combining ETOPO5 (National Geophysical Data Center – NGDC 1988) and BEDMAP in which sea floor topography is derived from the Smith and Sandwell (1997), ETOPO2 and ETOPO5 (NGDC, 1988). Ice shelf thickness was obtained from the BEDMAP gridded digital model of ice thickness (Lythe et al., 2001). Both surfaces were smoothed with a modified Shapiro filter which was designed to selectively smooth areas where the changes in the ice thickness or bottom bathymetry are large with respect to the total depth (Wilkin and Hedstrom, 1998).

The model was initialized with temperature and salinity fields from the January Levitus Word Ocean Data 1998 climatology. Under the ice shelf, stable theoretical vertical profiles of temperature and salinity were prescribed as initial conditions to avoid instabilities derived from excessive gravity waves at the beginning of the simulation. At the open northern boundary, the model uses the free-surface Chapman condition, the 2-D momentum Flather condition and the 3-D momentum and tracer radiation condition. Temperature and salinity from Levitus 1998 climatology are prescribed as lateral boundary conditions at the open northern boundary.

The simulation ran for 100 yr forced with the Normal Year Forcing Version 2.0 – COREv2 – (Large and Yeager, 2004). The Normal Year Forcing consists of a single annual cycle of all the data needed to force an ocean model. These data are representative of climatological conditions over decades and can be applied repeatedly

OSD
9, 3431–3449, 2012

for as many years of model integration as necessary (Large and Yeager, 2004). It includes a 6 hourly 10 m winds, sea level pressure, 10 m specific humidity and 10 m air temperature; the daily solar shortwave radiation flux and downwelling longwave radiation flux and the monthly precipitation. The air-sea interaction boundary layer is based on the bulk parameterization of Fairall et al. (1996). It was adapted from the Coupled Ocean-Atmosphere Response Experiment (COARE) algorithm for the computation of surface fluxes of momentum, sensible heat, and latent heat. Surface salinity is relaxed to Levitus climatology with a time scale of 180 days.

2.2 Water masses investigation

To assess water masses representation we have used the Optimum Multiparameter (OMP) analysis, introduced by Tomczak et al. (1981) as an extension of TS diagram techniques. From a broad perspective, OMP uses Sea Water Types – SWT to solve a linear system of mixture equations and determine the contribution of each water mass encountered at an oceanographic station. OMP assumes a linear mixture model with identical exchange coefficients for all properties (Eq. 1, Tomczak and Large, 1989; Tomczak, 1999; Leffanue and Tomczak, 2004).

$$\begin{cases} x_1\theta_1 + x_2\theta_2 + x_3\theta_3 + 0 & = \theta_{\text{Obs}} + R_\theta \\ x_1 S_1 + x_2 S_2 + x_3 S_3 + 0 & = S_{\text{Obs}} + R_S \\ x_1 O_1 + x_2 O_2 + x_3 O_3 - \Delta PV & = PV_{\text{Obs}} + R_O \\ x_1 + x_2 + x_3 + 0 & = 1 + R_{\text{mass}} \end{cases} \quad (1)$$

Scattered TS diagrams created with the 100-yr simulation results were compared against Ross Sea observed data from Orsi and Wiederwohl (2009). This allowed us to determine how ROMS was representing RS water masses and the numerical inherent biases. SWTs obtained from the TS diagrams were used to run OMP analysis and assess the spacial distribution of the main water masses found in the RS at a meridional cross section along the 165° W longitude.

OSD
9, 3431–3449, 2012

3 Results

Temperature and salinity data analyzed here refer to the last year of the 100-yr repeat annual cycle run and were were extracted from the cross section along the 165° W longitude (Fig. 2). First step was to build the scattered θ–S diagram (Fig. 3) in order to validate against observed data of Orsi and Wiederwohl (2009) and to check the water column structure represented by the model. First to be noticed was the overall structure quite similar to Orsi and Wiederwohl (2009), where the warm CDW, fresh AASW and the cold and salty SW can be fairly easy identified. As for most of numerical models, some biases are expected, no matter how good the simulation may be. In that sense, we must point that although the scattered θ–S presents the same triangular-shaped distribution as for Orsi and Wiederwohl (2009), the density field structure appears to be slightly less dense. Orsi and Wiederwohl (2009) suggest the CDW to be between 28.00 and 28.27 $kg\,m^{-3}$ neutral density surfaces, while our results show CDW between 27.80 and 27.90 $kg\,m^{-3}$ in agreement with Bergamasco et al. (2002b). Nevertheless, these results are consistent with Assmann et al. (2003) numerical experiments where MCDW is centered at the 27.80 $kg\,m^{-3}$ density layer, while our results show MCDW between the 27.75 and 27.80 $kg\,m^{-3}$ density layers.

3.1 OMP analysis

The scattered θ–S diagram created with the simulation results was used to obtain the SWTs for the OMP analysis (Table 1). Four water masses properties values were chosen considering both the observed data values and the intrinsic model bias in order to assess whether this numerical simulation was able to fully represent the water column structure for this sector of the Ross Sea. The OMP analysis results show water masses contribution maps (%) for AASW, CDW, SW and ISW (Fig. 4).

The AASW (Fig. 4a) occupies the surface layers along almost the whole cross section extent with salinity ranging from 34.30 to 34.45 and temperature centered at −1.0 °C, quite similar to Orsi and Wiederwohl (2009). Higher contribution values

OSD
9, 3431–3449, 2012

(> 90 %) will not show deeper than 200 m, except for the region near the shelf break where AASW reaches 500 m. Some AASW contribution is found in the upper layers over the continental shelf and close to the ice shelf, where sea ice formation will impact to transform it into SW to be the densest water mass around Antarctica (Orsi and Wiederwohl, 2009). The saltier MCDW originated by the CDW that eventually makes its way into the continental shelf is also part of this process. MCDW was not individually assessed in this work due to OMP numerical constraints, but an important interaction between AASW and CDW close to the shelf break may also be seen on OMP results (Fig. 4a, b).

As described by Worthington (1981) the CDW (Fig. 4b) appears as the most voluminous water mass, identified as a thick layer between the upper and colder AASW and the saltier AABW. As CDW is branched from ACC and carried southward by the Antarctic Coastal Current between 160° W and 165° W (Orsi and Wiederwohl, 2009), it is found at intermediate layers from northern limit of the cross sections 65° S to the continental slope at 75° S where it is incursion seems to be blocked by AASW near the shelf break. 34.68 salinity values are consistent with observational data, even though the model has represented CDW half degree colder (0.5 °C) than Orsi and Wiederwohl (2009) results around 1.0 °C. Small CDW contribution values at the bottom layers is probably related to the presence of AABW, although this water mass was not separated in this investigation.

Following Orsi and Wiederwohl (2009), we have established the upper limit of the SW (Fig. 4c) as the sudden scatter reduction at −1.85 °C, here centered at the 28.00 kg m^{-3} density layer a bit less dense than the 28.27 kg m^{-3} found by them. Here the SW seems to be more restrained to the salinity range of 34.65–34.90 compared to the $S > 34.50$ suggested by Orsi and Wiederwohl (2009), what makes these pretty consistent results. The densest SW is a trademark feature of the RS continental shelf and has its distribution pretty much constrained by the topography. OMP results show the SW spreading along the bottom layers of the shelf and clearly trapped by the risen shelf break. As discussed by many authors (Budillon et al., 2003; Holland et al., 2003; Muench et al.,

OSD
9, 3431–3449, 2012

2009; Orsi and Wiederwohl, 2009), the formation and export of the SW and its components occurs in pulses related to the polynyas recurrence. Another feature to be noticed is the very light contribution of the SW on the oceanic basin 4000 m, where the AABW takes place. Since the AABW results from the interaction of the SW and the CDW near the shelf break, these results suggest that the model may be reproducing important processes such as the AABW formation.

The ISW (Fig. 4d) occupies the bottom layers over the continental shelf and deepens towards the base of the ice shelf. Observational studies such as Budillon et al. (2003) point that the ISW spreads along the deep layers of the shelf, but over a thin layer of HSSW, which agrees with the believed formation process describe in Fig. 1 for the ISW. They discuss that from the 400 m depth to the bottom of the continental shelf there is essentially a mixture of HSSW and ISW that reach to shelf break to take part in the formation of the AABW. As suggested by Jacobs (2004) the ISW is defined as being colder than the sea water freezing point (at surface) with its formation occurring by means of melting at the RIS base. Although the ice shelf used in this simulation is static in time, its thermodynamic is enough to reproduce such melting processes. Here, as for Holland et al. (2003) numerical experiment, ISW definition includes all seawater colder than −1.95 °C (they used −1.90 °C) which may have lead ISW to be represented at both deep and bottom layers on the continental shelf.

4 Conclusions

The aim of this work was to assess the representation of the RS water masses with a regional ocean model with an active sea ice/ice shelf thermodynamic parametrization. Results suggest that the numerical investigations of such an isolated environment as the cavity beneath the RIS is not only feasible but much useful to understand the oceanographic processes related to water transformation under the ice shelves. Using the sea ice/ice shelf module we were able to reproduce the main thermohaline structure of the Ross Sea and to represent the main water masses: AASW, CDW, SW

OSD
9, 3431–3449, 2012

and ISW. These results are consistent with observations (Bergamasco et al., 2002a; Budillon et al., 2003; Orsi and Wiederwohl, 2009).

AASW was represented at the surface layers with salinity ranging from 34.30 to 34.45 and temperature centered at −1.0 °C. The warmer (0.5 °C) and saltier (34.68) CDW was represented as the most voluminous water mass spreading along intermediate layers, following the slope and reaching the outer portion of the shelf break. The SW appeared ate the bottom layers of the continental shelf, trapped by topography but still able to reach the shelf break with its characteristic low temperature (−1.85 °C) and high salinity (34.65–34.90). Finally the model was also able to represent the supercooled ISW with temperatures below −1.95 °C. These are remarkable results, since SW and its components are the most important water masses in the RS involved in the deep world ocean ventilation as they will interact with CDW to form the AABW. OMP analysis has provided a good spacial description of the RS water masses and works as an objective method for characterizing polar oceans. Since we have used only salinity and temperature as input for OMP only three water masses could be separated. We are currently using potential vorticity as an additional input to the OMP method which results in the identification of 4 water masses. Moreover, this investigation constitutes a starting point to further experimentations: first applying an interannual forcing to investigate the temporal evolution of water masses; secondly improving the ice shelf physics in the code.

Acknowledgements. To Virna Meccia for providing great help setting this experiment up and running, CNPq, FAPESP, CAPES and INCT-Criosfera.

References

Assmann, K., Hellmer, H., and Beckmann, A.: Seasonal variation in circulation and water mass distribution on the Ross Sea continental shelf, Antarct. Sci., 15, 3–11, 2003. 3433, 3434, 3438

OSD
9, 3431–3449, 2012

Bergamasco, A., Defendi, V., and Meloni, R.: Some dynamics of water outflow from beneath the Ross Ice Shelf during 1995 and 1996, Antarct. Sci., 14, 74–82, 2002a. 3434, 3441
Bergamasco, A., Defendi, V., Zambianchi, E., and Spezie, G.: Evidence of dense water overflow on the Ross Sea shelf-break, Antarct. Sci., 14, 271–277, 2002b. 3438
Bergamasco, A., Defendi, V., Budillon, G., and Spezie, G.: Downslope flow observations near Cape Adare shelf-break, Antarct. Sci., 16, 199–204, 2004. 3433, 3434
Bromwich, D. and Kurtz, D.: Katabatic wind forcing of the Terra Nova Bay polynya, J. Geophys. Res., 89, 3561–3572, 1984. 3434
Budgell, W.: Numerical simulation of ice–ocean variability in the Barents Sea region, Ocean Dynam., 55, 370–387, 2005. 3435
Budillon, G. and Spezie, G.: Thermohaline structure and variability in the Terra Nova Bay polynya, Ross Sea, Antarct. Sci., 12, 493–508, 2000. 3433, 3434
Budillon, G., Tucci, S., Artegiani, A., and Spezie, G.: Water Masses and Suspended Matter Characteristics of the Western Ross Sea, Ross Sea Ecology, Springer, Berlin, 63–81, 1999. 3434
Budillon, G., Pacciaroni, M., Cozzi, S., Rivaro, P., Catalano, G., Ianni, C., and Cantoni, C.: An optimum multiparameter mixing analysis of the shelf waters in the Ross Sea, Antarct. Sci., 15, 105–118, 2003. 3433, 3439, 3440, 3441
Dinniman, M., Klinck, J., and Smith Jr., W.: Influence of sea ice cover and icebergs on circulation and water mass formation in a numerical circulation model of the Ross Sea, Antarctica, J. Geophys. Res., 112, C11013, doi:10.1029/2006JC004036, 2007. 3436
Fairall, C., Bradley, E., Rogers, D., Edson, J., and Youngs, G.: Bulk parameterization of air–sea fluxes for Tropical Ocean-Global Atmosphere Coupled-Ocean Atmosphere Response, J. Geophys. Res., 101, 3747–3764, 1996. 3437
Gordon, A.: Interocean exchange of thermocline water, J. Geophys. Res., 91, 5037–5046, 1986. 3432
Gordon, A. and Tchernia, P.: Waters of the continental margin off Adelie Coast, Antarctica, Antarct. Oceanol., 2, 59–69, 1972. 3434
Holland, D. and Jenkins, A.: Modeling thermodynamic ice–ocean interactions at the base of an ice shelf, J. Phys. Oceanogr., 29, 1787–1800, 1999. 3436
Holland, D. and Jenkins, A.: Adaptation of an isopycnic coordinate ocean model for the study of circulation beneath ice shelves, Mon. Weather Rev., 129, 1905–1927, 2001. 3435

OSD
9, 3431–3449, 2012

Holland, D., Jacobs, S., and Jenkins, A.: Modelling the ocean circulation beneath the Ross Ice Shelf, Antarct. Sci., 15, 13–23, 2003. 3439, 3440
Hunke, E. and Dukowicz, J.: The elastic-viscous-plastic sea ice dynamics model in general orthogonal curvilinear coordinates on a sphere-incorporation of metric terms, Mon. Weather Rev., 130, 1848–1865, 2002. 3435
Jacobs, S.: Bottom water production and its links with the thermohaline circulation, Antarct. Sci., 16, 427–437, 2004. 3433, 3434, 3440
Jacobs, S., Amos, A., and Bruchhausen, P.: Ross Sea oceanography and Antarctic bottom water formation, in: Deep Sea Research and Oceanographic Abstracts, Vol. 17, Elsevier, Pergamon Press, UK, 935–962, 1970. 3434
Kurtz, D. and Bromwich, D.: A recurring, atmospherically forced polynya in Terra Nova Bay, in: Oceanology of the Antarctic Continental Shelf, edited by: Jacobs, S. S., Antarctic Research Series 43, American Geophysical Union, Washington, DC, 177–201, 1985. 3434
Large, W. and Yeager, S.: Diurnal to decadal global forcing for ocean and sea-ice models: the data sets and flux climatologies, National Center for Atmospheric Research, 2004. 3436, 3437
Leffanue, H. and Tomczak, M.: Using OMP analysis to observe temporal variability in water mass distribution, J. Mar. Syst., 48, 3–14, 2004. 3437
Lythe, M. B., Vaughan, D. G., and the BEDMAP Consortium: BEDMAP: a new ice thickness and subglacial topographic model of Antarctica, J. Geophys. Res., 106, 11335–11351, 2001. 3436
Mellor, G. and Kantha, L.: An ice–ocean coupled model, J. Geophys. Res., 94, 10937–10954, doi:10.1029/JC094iC08p10937, 1989. 3435
Muench, R., Padman, L., Gordon, A., and Orsi, A.: A dense water outflow from the Ross Sea, Antarctica: mixing and the contribution of tides, J. Mar. Syst., 77, 369–387, 2009. 3434, 3439
Orsi, A. and Wiederwohl, C.: A recount of Ross Sea waters, Deep-Sea Res. Pt. II, 56, 778–795, 2009. 3437, 3438, 3439, 3440, 3441
Orsi, A., Jacobs, S., Gordon, A., and Visbeck, M.: Cooling and ventilating the abyssal ocean, Geophys. Res. Lett, 28, 2923–2926, 2001. 3433
Orsi, A., Smethie Jr., W., and Bullister, J.: On the total input of Antarctic waters to the deep ocean: a preliminary estimate from chlorofluorocarbon measurements, J. Geophys. Res, 107, 3122, doi:10.1029/2001JC000976, 2002. 3433
Rintoul, S.: South Atlantic interbasin exchange, J. Geophys. Res., 96, 2675–2692, 1991. 3432

OSD
9, 3431–3449, 2012

Smethie, W., Jacobs, S. and Jacobs, S: Circulation and melting under the Ross Ice Shelf: estimates from evolving CFC, salinity and temperature fields in the Ross Sea, Deep-Sea Res. Pt. I, 52, 959–978, 2005. 3433

Smith, W. and Sandwell, D.: Global sea floor topography from satellite altimetry and ship depth soundings, Science, 277, 1956–1962, 1997. 3436

Song, Y. and Haidvogel, D.: A semi-implicit ocean circulation model using a generalized topography-following coordinate system, J. Comput. Phys., 115, 228–244, 1994. 3434, 3435

Tomczak, M.: Some historical, theoretical and applied aspects of quantitative water mass analysis, J. Mar. Res., 57, 275–303, 1999. 3437

Tomczak, M. and Large, D.: Optimum multiparameter analysis of mixing in the thermocline of the eastern Indian Ocean, J. Geophys. Res., 94, 16141–16149 doi:10.1029/JC094iC11p16141, 1989. 3437

Tomczak Jr., M.: A multi-parameter extension of temperature/salinity diagram techniques for the analysis of non-isopycnal mixing, Prog. Oceanogr., 10, 147–171, 1981. 3437

Wilkin, J. and Hedstrom, K.: User's manual for an orthogonal curvilinear grid-generation package, Institute of Marine and Coastal Sciences, Rutgers University, available at: http://www.marine.rutgers.edu/po/tools/gridpak/grid_manual.ps.gz, last access: 11 August 2004,1998. 3435, 3436

Worthington, L.: The water masses of the world ocean: some results of a fine-scale census, in: Evolution of Physical Oceanography: Scientific Surveys in Honor of Henry Stommel, edited by: Warren, B. A. and Wunsch, C., MIT Press, Cambridge, 6–41, 1981. 3439

OSD
9, 3431–3449, 2012

Table 1. Sea Water Types derived from TS diagram.

Water Mass	Salinity	Temperature
AASW	34.37	−1.0
SW	34.78	< −1.85
ISW	34.78	< −1.95
CDW	34.68	0.5

OSD
9, 3431–3449, 2012

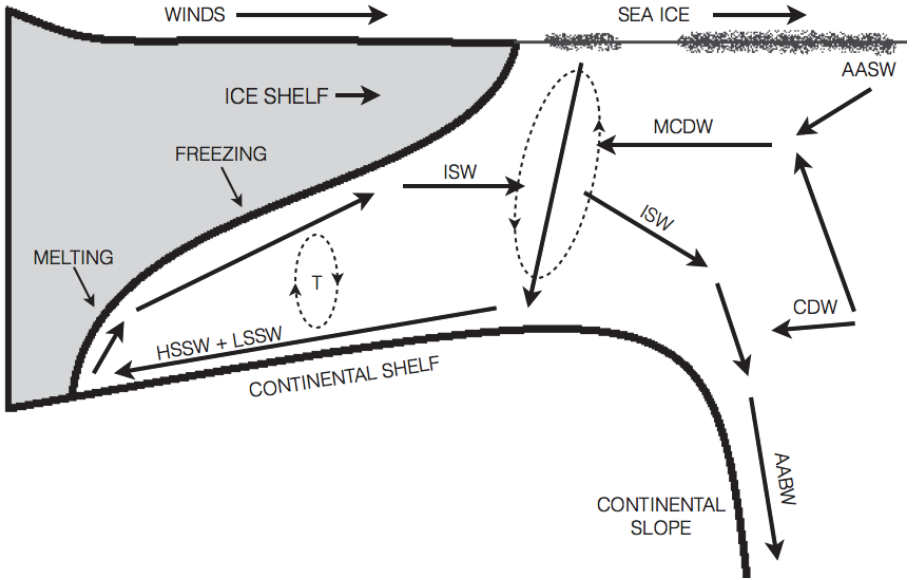

Fig. 1. Schematic representation of the circulation under the Ross Sea Ice Shelf. AASW: Antarctic surface water, CDW: circumpolar deep water, MCDW: modified circumpolar water, LSSW: low salinity shelf water, HSSW: high salinity shelf water, ISW: ice shelf water, AABW: Antarctic bottom water. T refers to tidal mixing.

OSD
9, 3431–3449, 2012

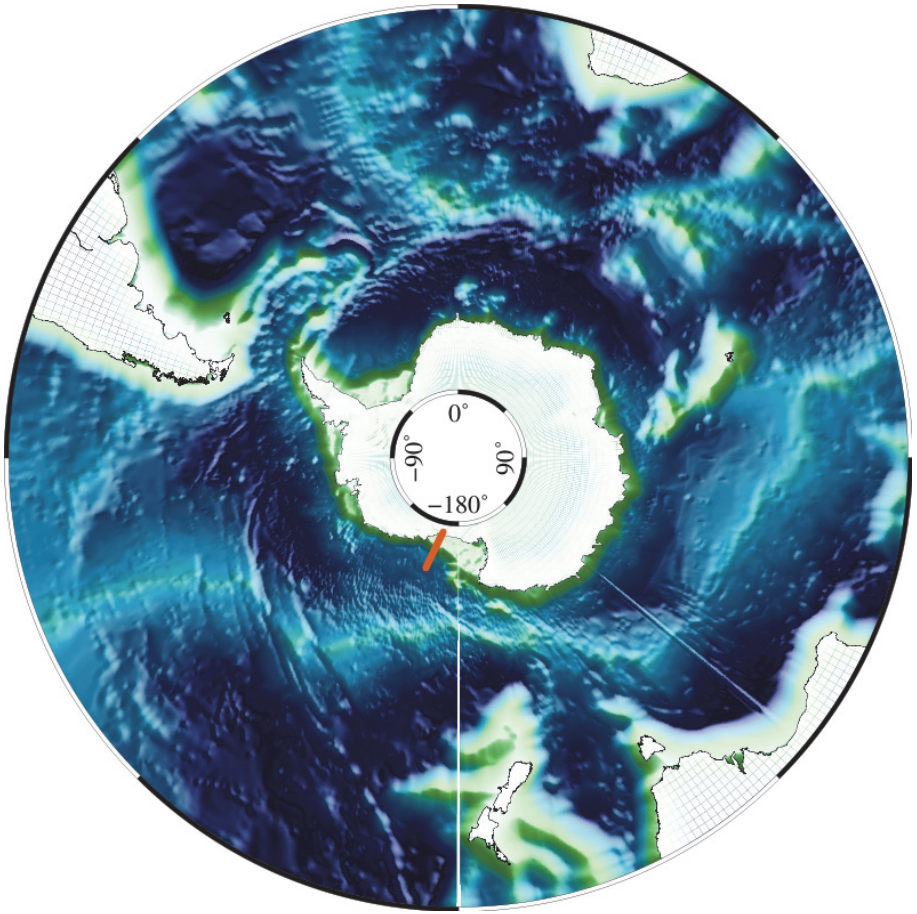

Fig. 2. Simulation domain – variable resolution grid reaching less than 5 km over the continental shelf. The orange line marks the cross section analyzed.

OSD
9, 3431–3449, 2012

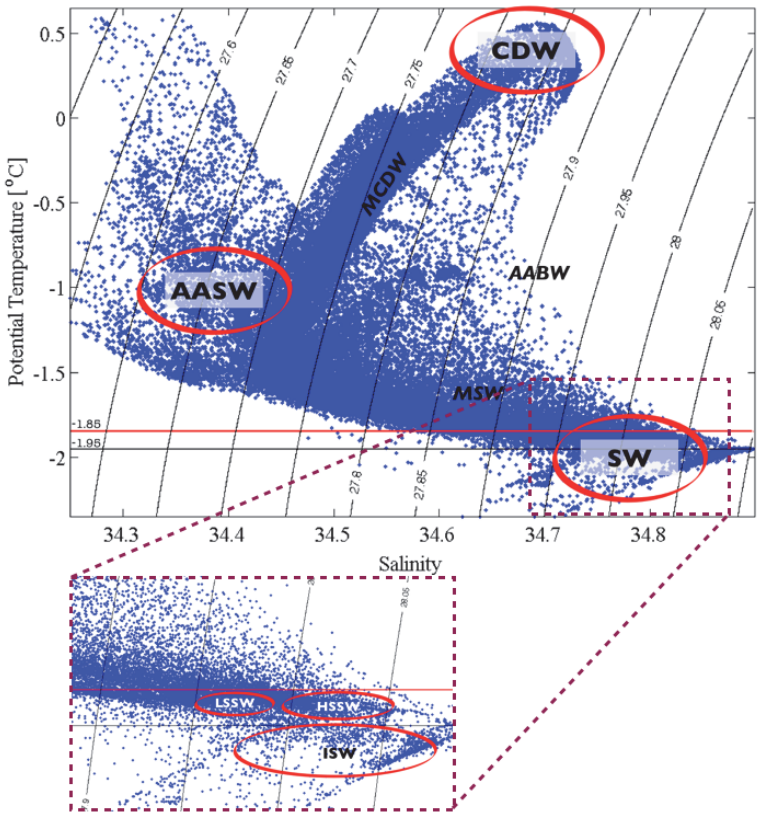

Fig. 3. Scattered *TS* diagram created with the simulation results showing the main Ross Sea water Masses. AASW: Antarctic surface water, CDW: circumpolar deep water, MCDW: modified circumpolar water, AABW: Antarctic bottom water, MSW: modified shelf water, SW: shelf water, LSSW: low salinity shelf water, HSSW: high salinity shelf water, ISW: ice shelf water.

OSD
9, 3431–3449, 2012

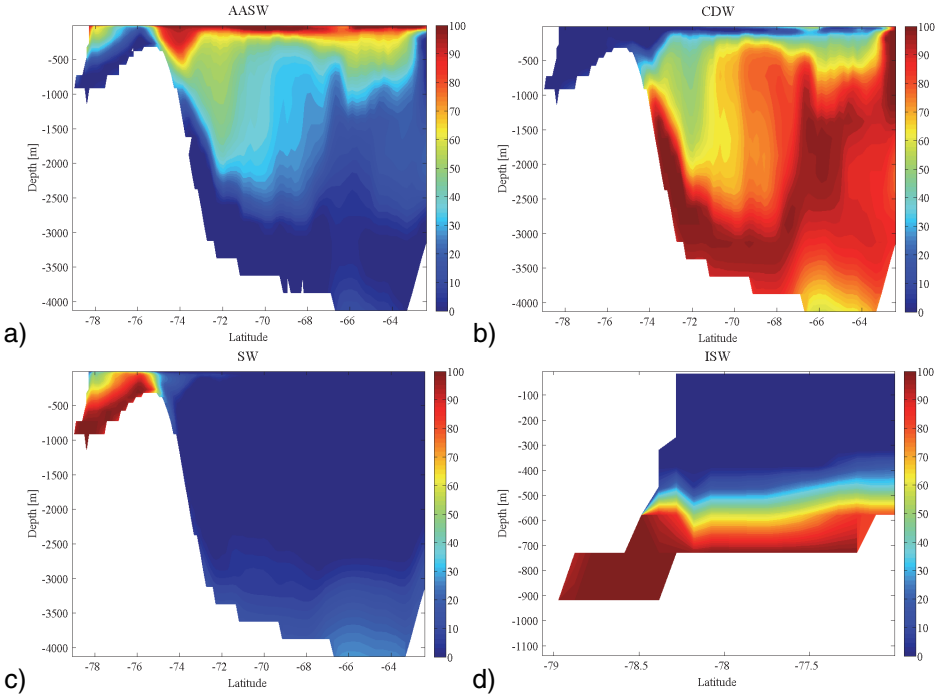

Fig. 4. (a) Antarctic surface water (AASW) spacial contribution (%) at the meridional section along the 165° W Latitude. **(b)** Circumpolar deep water (CDW) spacial contribution (%) at the meridional section along the 165° W Latitude. **(c)** Shelf water (SW) spacial contribution (%) at the meridional section along the 165° W Latitude. **(d)** Ice shelf water (ISW) spacial contribution (%) at the meridional section along the 165° W Latitude.

OSD
9, 3431–3449, 2012